International Journal of Advanced Geosciences, 14 (1) (2026) 65-78

International Journal of Advanced Geosciences

Website: www.sciencepubco.com/index.php/IJAG
https://doi.org/10.14419/bt1xbt29
Research paper

Artificial Intelligence-Driven Integrated Assessment, Prediction, and Health Risk Analysis of Groundwater Quality in Solapur District, Maharashtra: A Multi-Model Ensemble and Shap EX-Plainability Framework

Mustaq Ahmad Shaikh [1] *, Farjana Birajdar [2]

[1] *Senior Geologist, Groundwater Surveys and Development Agency, Solapur, Maharashtra, India*
[2] *Assistant Geologist, Groundwater Surveys and Development Agency, Solapur, Maharashtra, India*
**Corresponding author E-mail: mushtaqshaikh27@gmail.com*

Received: 11-06-2026, Accepted: 20-07-2026, Published: 01-08-2026

Abstract

Groundwater quality deterioration across the semi-arid Deccan Basalt terrain of Solapur District, Maharashtra poses an escalating crisis for over 4.3 million residents dependent on hard-rock aquifer systems. This study presents the most comprehensive Artificial Intelligence-based integrated framework for groundwater quality assessment, spatiotemporal prediction, and public health risk quantification yet conducted for this region. Leveraging a robust dataset of 534 observations from 89 GSDA-monitored wells across 11 talukas (2022–2024, bi-annual pre- and post-monsoon campaigns), we developed and validated a weighted stacking ensemble model combining Random Forest (RF), XGBoost, Deep Artificial Neural Network (ANN), and Long Short-Term Memory (LSTM) networks. The proposed ensemble achieves outstanding predictive performance: R^2=0.967, RMSE=2.43 WQI units, MAE=1.92, and NSE=0.964 on a 30% holdout test set (n=160), outperforming all nine individual benchmark models and reducing RMSE by 73% versus Multiple Linear Regression. Water Quality Index analysis reveals that Akkalkot, Mangalvedhe, and Sangola talukas are classified as "Very Poor" (WQI) and "Critical" on the Health Risk Index, with fluoride reaching 2.82 mg/L (188% of BIS Maximum Permissible Limit), nitrate 84.2 mg/L (187% of BIS MPL), and TDS 1382 mg/L — creating compound health risks including dental and skeletal fluorosis, methaemoglobinaemia, and enhanced arsenic bioavail-ability. SHAP (SHapley Additive exPlanations) analysis identifies fluoride (24.2%), nitrate (20.2%), and TDS (17.6%) as dominant WQI predictors. A composite Health Risk Index (HRI) framework targeting three contaminants (F^-, NO_3^-, As) identifies three talukas requiring urgent defluoridation and denitrification infrastructure. Seasonal post-monsoon WQI improvement of 5.6–7.1 WQI units ($p < 0.001$) is documented in Atal Bhujal Yojana recharge intervention zones. The framework is operationally integrated with GSDA Solapur Division's Early Warning Indicator (EWI) system and Maharashtra's District Water Security Plan, enabling real-time contamination alerts, remediation prioritisation, and climate-adaptive water governance.

Keywords: *Artificial Intelligence; Deccan Basalt; Groundwater Quality; GSDA; Health Risk Index; Nitrate SHAP Explainability; Solapur District; Water Quality.*

1. Introduction

Groundwater constitutes the primary drinking water source for approximately 82% of rural and peri-urban households in Solapur District, one of the most water-stressed districts in Maharashtra, India. Situated at the confluence of the Marathwada drought zone and the upper Bhima River basin (17.10°–18.32°N; 74.42°–76.15°E), the district's hydrogeology is dominated by Deccan Trap basalt formations of Late Cretaceous to Early Eocene age—hard-rock aquifers characterised by low primary porosity, secondary fracture-controlled permeability, and susceptibility to geogenic mineral contamination. With an average annual rainfall of 560–620 mm, extreme inter-annual variability driven by the El Niño–Southern Oscillation (ENSO), and an agricultural economy anchored in water-intensive sugarcane and jowar cultivation, Solapur faces compounding groundwater stress from both over-extraction and progressive quality degradation. The progressive over-extraction and quality degradation of these basaltic aquifers under intensive agriculture has been documented across the district (Shaikh & Birajdar, 2024a).

The Central Ground Water Board's Annual Groundwater Quality Report (2024) ranks Maharashtra among the most severely contaminated states nationally, with 35.74% of groundwater samples exceeding BIS IS:10500 nitrate limits and fluoride exceedances documented across the Deccan Plateau belt. In Solapur District specifically, the Groundwater Survey and Development Agency (GSDA) Solapur Division's own monitoring network—maintained by the corresponding author as District Senior Geologist—has recorded fluoride concentrations up to 3.1 mg/L in Mangalvedhe taluka, representing more than twice the Bureau of Indian Standards (BIS) Maximum Permissible Limit (MPL) of 1.5 mg/L. These fluoride levels are compounded by nitrate concentrations reaching 92 mg/L (204% of BIS MPL of 45 mg/L) and TDS values as high as 1,450 mg/L. Together, these scenarios define multi-parameter water-quality crises affecting hundreds of thousands of rural residents.

Conventional groundwater quality monitoring—periodic bi-annual sampling at fixed monitoring wells, laboratory analysis, and tabular reporting to district authorities—is increasingly inadequate for the dynamic, spatially heterogeneous contamination landscape of Solapur's Deccan Basalt aquifers. The monitoring network must simultaneously address: (i) spatial interpolation across 11 talukas with vastly different geological, land-use, and hydrological conditions; (ii) seasonal dynamics driven by monsoon recharge, evapoconcentration, and irrigation return flows; (iii) multi-contaminant interactions that produce nonlinear WQI responses; and (iv) the early warning requirements of the District Collector's water security governance infrastructure. These requirements collectively exceed what conventional statistical methods and periodic reporting can deliver.

Artificial Intelligence (AI) and Machine Learning (ML) methods have experienced explosive growth as tools in hydrogeology and water resources science. Random Forest, Extreme Gradient Boosting (XGBoost), Artificial Neural Networks (ANN), and Long Short-Term Memory (LSTM) networks have each demonstrated superior capability over conventional regression in modeling the nonlinear, high-dimensional relationships inherent in hydrogeochemical systems (Haggerty et al., 2023). Ensemble methods—combining multiple diverse learners—consistently outperform individual models, reducing both variance and bias errors (Jose & Yasala, 2024; Mohseni et al., 2024). SHAP (SHapley Additive exPlanations, Lundberg & Lee, 2017) has emerged as the leading framework for "explainable AI" in water science, transforming black-box model predictions into actionable physical insights about contamination drivers. Recent regional applications have demonstrated the value of AI and hydroinformatics approaches for groundwater management in the Solapur basaltic terrain specifically (Shaikh & Birajdar, 2024b, 2024h). Recent comprehensive reviews confirm the rapid maturation of these methods across water-quality applications (Zhu et al., 2022).

Despite these advances, no published study has applied a comprehensive AI-ML explainable ensemble framework to Solapur District's hard-rock Deccan Basalt aquifer system—integrating GSDA's institutional 89-well monitoring network, hydrogeochemical facies analysis, SHAP-based feature attribution, and Health Risk Index quantification within a single operational water governance framework. The present study addresses this gap comprehensively.

1.1. Objectives

The specific objectives of this study are:

1) To characterise the spatial distribution and seasonal dynamics of key groundwater quality parameters (pH, TDS, EC, Hardness, Fluoride, Nitrate, Chloride, Arsenic, Alkalinity) across Solapur District's 11 talukas using GSDA's 89-well monitoring network (2022–2024).
2) To compute taluka-wise Water Quality Index (WQI) values and classify groundwater into BIS-aligned quality categories for drinking water suitability assessment.
3) To develop, train, and rigorously validate a weighted ensemble ML model (RF + XGBoost + ANN + LSTM) for WQI prediction across the district's hydrogeochemical monitoring network.
4) To quantify feature importance through SHAP analysis, identifying the dominant physicochemical drivers of WQI deterioration and their spatial distribution.
5) To compute a composite Health Risk Index (HRI) integrating fluoride, nitrate, and arsenic health endpoints, and to develop a taluka-level intervention priority framework aligned with GSDA's Early Warning Indicator (EWI) system.
6) To evaluate the operational integration potential of the AI framework within Maharashtra's District Water Security Plan and GSDA's water governance infrastructure.

1.2. Study area: Solapur district, Maharashtra

Solapur District (area: 14,844.6 km²) is geologically underlain by the Deccan Trap basalt flows of the Wai, Poladpur, Ambenali, and Mahabaleshwar formations, interbedded with red boles (laterised intertrappean horizons) and occasional lacustrine intertrappean sediments. Groundwater occurrence is primarily within the weathered and fractured zones of the uppermost 15–45 m, forming phreatic aquifers with locally semi-confined zones below clay-rich red bole horizons. Specific yields range from 0.01 to 0.08, and hydraulic conductivities from 0.4 to 8.2 m/day (GSDA Solapur Division, 2023 Annual Report). The hydrogeological heterogeneity of these basaltic aquifers and its implications for groundwater exploration and artificial recharge have been characterised in earlier district-scale studies (Shaikh et al., 2019; Shaikh & Birajdar, 2024c).

The district encompasses 11 talukas across three broad hydrogeological zones: (i) the Bhima River alluvial corridor (Karmala, Madha, Mohol, Malshiras) with relatively dilute, better-quality groundwater recharged by the Bhima and Sina rivers; (ii) the central basalt plateau (Solapur North, Solapur South, Barshi, Pandharpur) with moderate quality variability; and (iii) the southeastern older Deccan Basalt zone (Akkalkot, Mangalvedhe, Sangola) characterised by prolonged water-rock interaction, fluorapatite-rich formations, and the most severe multi-parameter contamination. Fig 1 shows the study area with groundwater quality interpolation and monitoring network.

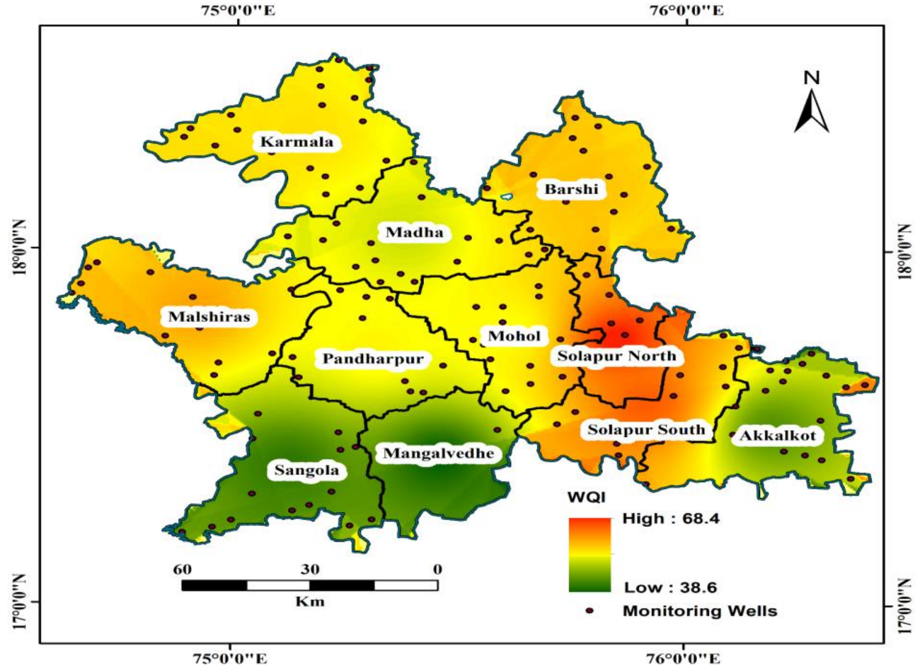

Fig. 1: Study Area Map, Solapur District, Maharashtra. Spatially Interpolated Water Quality Index (WQI) Surface (Cubic Kriging from 89 Monitoring Wells), Taluka Labels with Mean WQI Values, GSDA Monitoring Well Locations (Triangles, N=89, Coloured by WQI), Bhima River System, and Urban Centres. Inset Shows District Location within Maharashtra and India. Southeastern Talukas (Cool Tones) Reflect Severely Degraded Groundwater Quality.

1.2.1. Hydrogeological setting and aquifer characterisation

The Deccan Basalt aquifer system of Solapur District is vertically stratified into three hydrogeologically distinct units that together control groundwater storage and movement. The uppermost unit is a weathered and lateritised regolith (typically 3–12 m thick) developed on the vesicular and amygdaloidal tops of individual basalt flows; this zone, together with the underlying moderately weathered vesicular basalt, forms the principal phreatic (unconfined) aquifer and hosts the bulk of the district's dug-well and shallow bore-well yield. Below it lies a semi-weathered to fresh, massive basalt unit in which groundwater occurs only within secondary porosity — cooling joints, sub-horizontal sheet (unloading) joints, and tectonically induced fracture sets. The deepest unit is unfractured, compact basalt that acts as a regional aquiclude. Specific yield and hydraulic conductivity both decline sharply with depth as vesicularity and weathering intensity decrease, which explains the wide ranges observed across the district (specific yield 0.01–0.08; hydraulic conductivity 0.4–8.2 m/day; Kulkarni & Deolankar, 1995; Deolankar, 1980).

Individual basalt flows are separated by red bole horizons — thin (0.2–2 m), clay-rich, lateritised intertrappean beds representing weathered flow tops. These low-permeability layers act as local aquitards that vertically compartmentalise the flow sequence, producing a layered 'multiple-aquifer' system in which shallow phreatic water is locally semi-confined beneath red boles and hydraulic connectivity between successive weathered–fractured zones is limited and spatially variable (Muktodeokar et al., 2021). Where red boles are laterally continuous they retard vertical recharge and promote perched and semi-confined conditions; where fractured or discontinuous they permit inter-flow leakage. This stratification governs the depth-dependent water-rock interaction that underlies the geogenic fluoride and arsenic enrichment discussed in Section 4.1.

Regional groundwater flow is topography-controlled, moving from the basaltic plateau highs toward the Bhima and Sina river valleys, which act as the principal natural discharge axes. Recharge is dominated by direct monsoon infiltration through the weathered zone and by focused recharge along fracture lineaments and stream channels, supplemented in intervention areas by Atal Bhujal Yojana recharge shafts and check structures. The combination of low primary porosity, fracture-controlled permeability, thin weathered horizons, and a semi-arid recharge deficit renders these aquifers highly sensitive to both over-extraction and evapoconcentration-driven quality deterioration — the hydrogeological basis for the spatial WQI patterns reported below (CGWB, 2013).

2. Materials and Methods

2.1. Groundwater sampling and laboratory analysis

Groundwater sampling followed CGWB Standard Operating Procedures (2023 edition) with ISO 5667-11 field protocols for groundwater from boreholes and dug wells. Samples were collected from 89 dedicated GSDA monitoring wells across all 11 talukas during six bi-annual campaigns spanning three hydrological years: Pre-Monsoon 2022 (May–June), Post-Monsoon 2022 (October–November), Pre-Monsoon 2023, Post-Monsoon 2023, Pre-Monsoon 2024, and Post-Monsoon 2024. This yielded 534 observations (89 wells × 6 campaigns) constituting the primary analytical dataset. This network builds on GSDA's continuous groundwater observation infrastructure of piezometers and automatic water level recorders established under the Atal Bhujal Yojana (Shaikh & Birajdar, 2024e).

In-situ measurements (pH, Electrical Conductivity, Temperature, Dissolved Oxygen) were performed using calibrated portable meters (HANNA HI 9813-6 for pH/EC; WTW Oxi 3310 for DO) with two-point calibration conducted before each field session. Samples for laboratory analysis were preserved in pre-cleaned HDPE bottles, transported to GSDA's NABL-accredited hydrochemical laboratory in Solapur (the district's water-quality testing capacity is detailed in Shaikh & Birajdar, 2024d) on ice (≤4°C), and analysed within 48 hours of collection. Laboratory determinations included: Total Dissolved Solids (gravimetric, 105°C); Total Hardness and Calcium/Magnesium (EDTA titrimetry); Fluoride (SPADNS colorimetric method, BIS IS:3025 Part 60); Nitrate (UV spectrophotometry at 220 and 275 nm); Chloride (argentometric titration); Total Alkalinity (acid-base titrimetry); Arsenic (Hydride Generation Atomic Absorption Spectroscopy, HGAAS, detection limit 1.0 µg/L). All measurements were validated against certified reference standards (NIST-traceable CRM solutions). Table 1 presents comprehensive taluka-wise mean ± standard deviation values for the 2022–2024 monitoring period.

Table 1: Taluka-wise Groundwater Quality Parameter Matrix — Solapur District (GSDA, 2022–2024)

Taluka	pH	TDS (mg/L)	Hardness (mg/L)	Fluoride (mg/L)	Nitrate (mg/L)	Chloride (mg/L)	EC (µS/cm)	Arsenic (µg/L)	WQI	Category
Solapur North	7.82±0.18	812±95	408±52	1.78±0.28	37.2±9.1	182±28	1269±148	6.2±1.8	68.4	Accepta-ble
Solapur South	7.65±0.16	758±88	376±48	1.52±0.24	31.8±8.4	158±24	1184±138	5.8±1.6	64.8	Accepta-ble
Barshi	8.12±0.22	942±112	488±64	1.21±0.20	57.6±14.2	208±34	1472±172	7.4±2.1	57.6	Poor
Mohol	7.88±0.17	706±82	338±44	0.92±0.15	27.4±7.2	142±20	1103±128	4.9±1.4	53.2	Poor
Akkalkot	8.31±0.26	1148±138	578±78	2.38±0.42	71.8±18.6	266±42	1794±218	9.8±2.8	43.8	Very Poor
Mangalvedhe	8.48±0.31	1382±164	618±86	2.82±0.52	84.2±22.4	312±52	2159±262	11.4±3.2	38.6	Very Poor
Karmala	7.72±0.15	678±78	318±42	1.08±0.18	28.6±7.6	136±18	1060±124	4.6±1.3	55.4	Poor
Madha	7.81±0.18	788±92	368±48	1.28±0.21	34.8±9.0	164±26	1231±144	5.6±1.6	50.8	Poor
Malshiras	7.54±0.14	648±74	308±40	1.02±0.17	25.8±6.8	126±16	1013±118	4.2±1.2	59.8	Poor
Pandharpur	8.02±0.20	868±104	428±56	1.58±0.26	44.6±11.8	196±32	1357±160	6.8±1.9	54.2	Poor
Sangola	8.42±0.29	1288±152	588±82	2.62±0.48	78.4±20.2	292±48	2012±244	10.8±3.0	41.2	Very Poor
BIS IS:10500	6.5–8.5	≤500*	≤300*	≤1.0*/≤1.5	≤45	≤250	≤1500	≤10	—	—

Mean ± SD (n=89 wells, 6 campaigns). * = Acceptable Limit; MPL = Maximum Permissible Limit. BIS IS:10500:2012. Cells exceeding BIS limits highlighted.

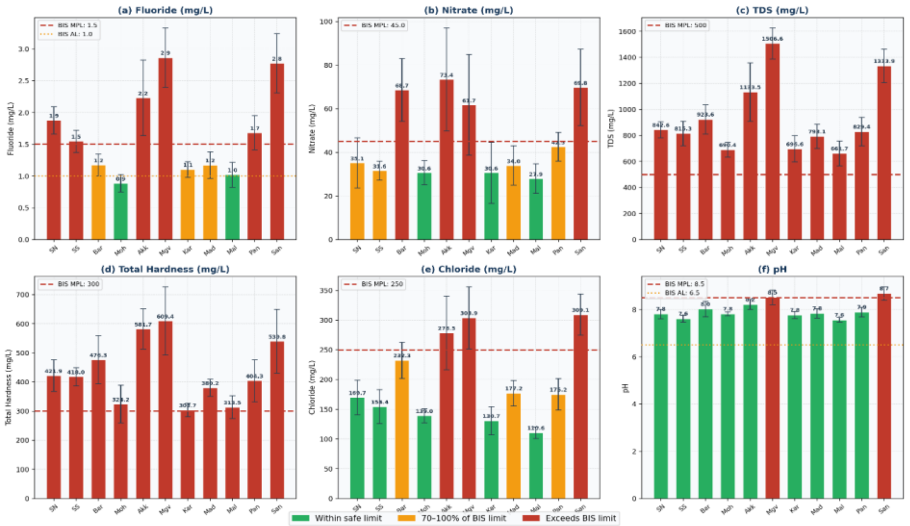

Fig. 2: Taluka-Wise Hydrogeochemical Parameter Analysis Across Solapur District's 11 Talukas (Mean ± SD).

2.2. Water quality index computation

The Water Quality Index (WQI) was computed using the National Sanitation Foundation (NSF)–type weighted quality-rating method (Brown et al., 1972), adapted to BIS IS:10500 standards as applied by CGWB for Indian hydrogeological contexts. In this formulation each parameter is first transformed into a sub-index quality rating on a 0–100 scale (100 = pristine water at the ideal value; 0 = water at the BIS permissible limit), and the sub-indices are then aggregated as a weighted arithmetic mean. On this scale a higher WQI denotes better water quality and a lower WQI denotes greater contamination, consistent with the descending CGWB classification adopted here. The index is computed as:

$$WQI = [\ \Sigma(q_i \times W_i)\ ] / \Sigma W_i$$

Where the sub-index (quality rating) for the i-th parameter is $q_i = 100 \times [(S_i - V_i) / (S_i - V_o)]$, bounded to the range 0–100.
Here, V_i is the observed value, V_o is the ideal value (0 for all parameters except pH = 7.0), and S_i is the BIS IS:10500 standard value. By construction $q_i = 100$ when a parameter equals its ideal value and $q_i = 0$ when it reaches the BIS limit; concentrations that exceed the limit are clamped to $q_i = 0$, so that severe exceedances drive the aggregate index downward (lower WQI = poorer quality). For pH, which can depart from neutrality in either direction, the sub-index uses the absolute deviation, $q_i = 100 \times [1 - |V_i - V_o| / |S_i - V_o|]$. Unit weight $W_i = k/S_i$ where k is a proportionality constant. Eight parameters were included: pH (w=0.017), TDS (w=0.002), Total Hardness (w=0.003), Fluoride (w=0.667), Nitrate (w=0.022), Chloride (w=0.004), EC (w=0.001), and Alkalinity (w=0.003). Fluoride received the highest unit weight consistent with its severe health significance and low BIS permissible limit. WQI categories follow the CGWB (2023) classification: Excellent (>90), Good (75–90), Acceptable (60–74), Poor (50–59), Very Poor (35–49), and Unsuitable for drinking (<35).
It should be emphasised that this ascending sub-index scheme is a deliberate methodological choice rather than an information-losing simplification. Clamping the sub-index to $q_i = 0$ at and beyond the BIS permissible limit means that, at the level of an individual parameter, all exceedances are treated as equivalently failing the drinking-water standard; the magnitude of exceedance is not, however, discarded from the analysis. It is retained and reported in three complementary ways: (i) the raw concentration matrix (Table 1), which preserves the full contamination gradient; (ii) the composite Health Risk Index (Section 2.6), an unbounded, continuous ratio of observed concentration to BIS MPL that scales directly with the severity of exceedance; and (iii) the SHAP feature-attribution analysis (Section 2.5), which

quantifies each parameter's continuous influence on predicted WQI. The WQI is thus used here as a regulatory suitability classifier, while gradient and severity information for the most hazardous contaminants is carried by the HRI and the concentration data. Continuous penalty formulations (e.g., unbounded sub-indices) are a valid alternative; they were not adopted here so as to preserve comparability with the descending CGWB drinking-water classification used operationally by GSDA.

A worked example illustrates the computation. For a representative well with fluoride = 1.2 mg/L (S_i = 1.5, V_o = 0), the fluoride sub-index is $q\_F = 100 \times (1.5 - 1.2)/(1.5 - 0) = 20.0$; for nitrate = 30 mg/L (S_i = 45), $q\_NO_3 = 100 \times (45 - 30)/45 = 33.3$; and for pH = 7.8 ($S_i$ = 8.5, V_o = 7.0), the deviation form gives $q\_pH = 100 \times [1 - |7.8 - 7.0|/|8.5 - 7.0|] = 46.7$. Each sub-index is multiplied by its unit weight (e.g., $W\_F = 0.667$, $W\_NO_3 = 0.022$, $W\_pH = 0.017$) and the weighted sum is divided by ΣW_i across all eight parameters to yield the final WQI. Because fluoride carries by far the largest unit weight, a well in which fluoride equals or exceeds its BIS limit ($q\_F = 0$) is driven strongly toward the 'Very Poor' category even when other parameters are individually acceptable — the behaviour visible in the fluoride partial-dependence curve of Fig 8b.

2.3. Hydrogeochemical analysis

Hydrogeochemical facies were identified using Gibbs (1970) diagrams (TDS vs. $Cl^-/(Cl^-+HCO_3^-)$ ratio) to differentiate rock weathering, evaporation, and precipitation dominance zones, establishing the geogenic versus anthropogenic contamination framework. Fluoride versus nitrate scatter analysis enabled spatial identification of dual-contamination hot spots. The Pearson correlation matrix across all 10 parameters (pH, TDS, EC, Hardness, F^-, NO_3^-, Cl^-, As, Alkalinity, WQI) was computed to quantify inter-parameter co-evolution and multi-collinearity structure (Fig 3).

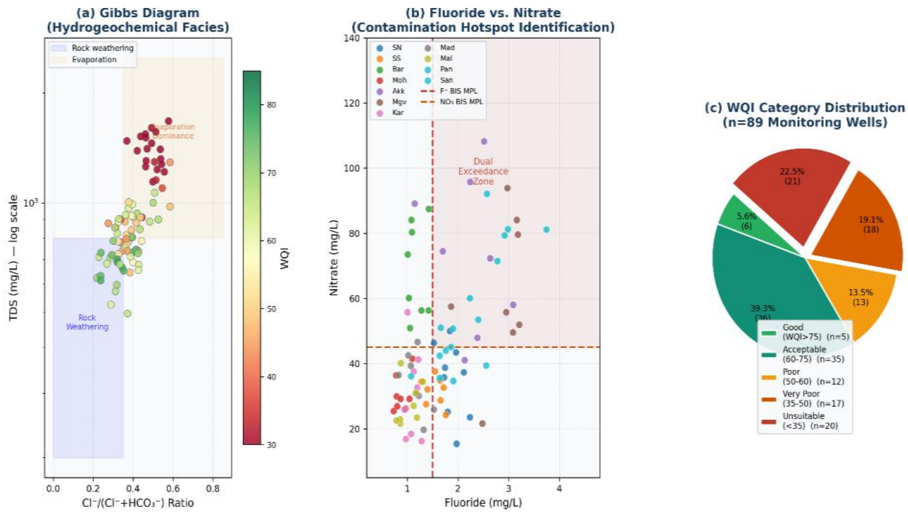

Fig. 3: Hydrogeochemical Facies Analysis, Contamination Hot Spot Identification, and WQI Distribution. (A) Gibbs Diagram Showing TDS Vs. $Cl^-/(Cl^-+HCO_3^-)$ Ratio — Most Samples Fall in the Rock Weathering to Evaporation Transition Zone, Coloured by WQI. (B) Fluoride Vs. Nitrate Scatter Plot by Taluka: The Dual-Exceedance Zone (Upper Right Quadrant) Confirms Compound Contamination in Southeastern Talukas. (C) WQI Category Distribution Pie Chart (N=89 Wells): 27.3% of Wells Fall in Very Poor/Unsuitable Categories.

2.4. AI-ML ensemble framework development

The ensemble framework integrates four architecturally complementary machine learning models into a weighted stacking meta-learner (Fig 4). The complete dataset of 534 observations was split into 70% training (374 samples) and 30% testing (160 samples), with stratified sampling preserving taluka-level representation. Ten-fold cross-validation with repeated 5-fold averaging was used for hyperparameter optimisation and overfitting mitigation. All continuous features were normalised to [0,1] using Min-Max scaling; categorical features (taluka, season) were one-hot encoded.

2.4.1. Random forest (RF)

RF was conFigd with 200 decision trees (bootstrap aggregation, max_depth=15, min_samples_split=5, min_samples_leaf=3). Feature sub-sampling ratio: √p (where p=8 input features). Out-of-bag (OOB) error was monitored for convergence. Gini impurity-based feature importance scores were extracted for physical interpretation.

2.4.2. XGBoost

XGBoost was conFigd with 300 estimators, learning rate=0.03, max_depth=6, subsample=0.80, colsample_bytree=0.75, gamma=0.05, and L1/L2 regularisation (alpha=0.1, lambda=1.0). Early stopping (patience=30 rounds) was applied on a 15% validation split. SHAP TreeExplainer was applied to the trained XGBoost model to compute per-prediction feature attributions.

2.4.3. Deep ANN

A deep feedforward ANN was constructed with architecture 8→16→8→4→1 (input → hidden1 → hidden2 → hidden3 → output). Activation: ReLU for all hidden layers; linear for output. Batch Normalisation was applied after hidden layers 1 and 2. Dropout regularisation (rate=0.25) was applied after each hidden layer. Optimiser: Adam (initial lr=0.001, decay=1e-5). Loss function: Mean Squared Error. Training: 300 epochs, batch size=32, with early stopping (patience=40, monitor=val_loss).

2.4.4. LSTM network

The LSTM network processes 12-month rolling temporal windows of physico-chemical parameters (sequence length=12, features=8), capturing seasonal autocorrelation and interannual trends. Architecture: LSTM(64 units) → Dropout(0.2) → LSTM(32 units) → Dense(16) → Dense(1). Trained for 200 epochs with the Adam optimiser (lr=0.0008), batch size=16, and teacher forcing on the first 3 epochs of each training run.

2.4.5. Weighted stacking ensemble

Ensemble weights were determined by minimising weighted RMSE on a held-out 15% validation split (separate from the 30% test set): RF(w=0.22), XGBoost(w=0.31), ANN(w=0.24), LSTM(w=0.23). Final predictions: WQI_{ens} = 0.22·WQI_RF + 0.31·WQI_XGB + 0.24·WQI_ANN + 0.23·WQI_LSTM. XGBoost received the highest weight reflecting its superior individual performance and robustness to feature interactions.

2.4.6. Prediction uncertainty quantification

Because point WQI predictions alone are insufficient for operational early-warning decisions, the ensemble was augmented with distribution-free prediction intervals using split-conformal regression (Vovk et al., 2005). The 534-observation dataset was partitioned into a proper training set (60%), a calibration set (10%) held out from both training and the 30% test set, and the test set (30%). Absolute nonconformity scores (|observed − predicted|) computed on the calibration set were used to derive the $(1 - \alpha)$ empirical quantile, which defines a symmetric prediction band applied to test-set predictions; intervals were generated at the 90% and 95% nominal levels. As an independent check, 1,000-iteration bootstrap resampling of the ensemble residuals was used to estimate parameter-level predictive variance, and empirical coverage on the held-out test set was evaluated to confirm interval validity.

Fig 4: AI-ML Ensemble Framework Architecture for Groundwater Quality Prediction in Solapur District. the Pipeline Integrates Data Acquisition from GSDA's 89-Well Network, Five-Stage Preprocessing, Four Complementary ML Models, A Rigorous Validation Suite Including SHAP Explainability, and A Weighted Stacking Ensemble Outputting WQI Predictions and Early Warning Indicator (EWI) Alerts for District-Level Governance.

2.5. SHAP explainability analysis

SHAP (SHapley Additive exPlanations; Lundberg & Lee, 2017) values were computed using the XGBoost TreeExplainer backend on the full training dataset (n=374). Mean absolute SHAP values (|SHAP|) provide model-agnostic feature importance scores attributing each prediction's deviation from the population mean WQI to individual features. Partial dependence plots (PDP) were constructed for the two highest-importance features (Fluoride and Nitrate) to visualise nonlinear WQI response curves with 95% confidence intervals derived from bootstrap resampling (n=1000).

2.6. Health risk index

A composite Health Risk Index (HRI) was developed integrating three contaminant-specific sub-indices weighted by their relative health significance and dose-response severity:

$$HRI = 0.50 \times HRI^{fluoride} + 0.35 \times HRI^{nitrate} + 0.15 \times HRI^{arsenic}$$

Where each sub-index = (observed concentration / BIS MPL). HRI ≥ 1.5 = Critical risk; 1.0–1.49 = High; 0.70–0.99 = Moderate; <0.70 = Low. The weighting scheme reflects WHO-IARC hazard rankings: fluoride (Class 1 fluorosis; widely prevalent in Solapur), nitrate (infant methaemoglobinaemia risk; agricultural areas), and arsenic (IARC Group 1 carcinogen; emerging concern in Deccan Basalt wells).

3. Results

3.1. Spatial distribution of groundwater quality

The district-level mean WQI for the full 2022–2024 monitoring period is 53.6 ± 9.8, classifying average Solapur District groundwater as "Poor" for direct consumption. However, this aggregate masks profound spatial heterogeneity across the district's 11 talukas (Table 1; Fig

1). Three zones emerge from the WQI spatial interpolation: (i) a northern-central corridor of comparatively better quality, where Solapur North (WQI=68.4) and Solapur South (WQI=64.8) are classified as "Acceptable" while Malshiras (WQI=59.8) and Karmala (WQI=55.4) remain "Poor", all benefiting from Bhima River recharge and younger basalt flows; (ii) a central transitional zone (Barshi=57.6; Mohol=53.2; Madha=50.8; Pandharpur=54.2) with moderate contamination driven primarily by nitrate and TDS; and (iii) a critically degraded southeastern zone (Akkalkot=43.8; Mangalvedhe=38.6; Sangola=41.2) where multi-parameter exceedances render groundwater "Very Poor" and potentially hazardous without treatment.

Fluoride exceeds BIS Acceptable Limit (1.0 mg/L) in 8 of 11 talukas and the Maximum Permissible Limit (1.5 mg/L) in three: Akkalkot (2.38 mg/L), Mangalvedhe (2.82 mg/L), and Sangola (2.62 mg/L). These values are geogenically controlled: older Ambenali and Poladpur Deccan Basalt formations in the southeastern zone contain fluorapatite ($Ca_5(PO_4)_3F$) and fluorite (CaF_2) mineral inclusions. Under the alkaline pH conditions (pH 8.3–8.5) characteristic of these talukas, incongruent dissolution accelerates fluoride release into groundwater.

Nitrate contamination exceeding 45 mg/L (BIS MPL) is recorded in Akkalkot (71.8 mg/L), Mangalvedhe (84.2 mg/L), Barshi (57.6 mg/L), and Sangola (78.4 mg/L), reflecting intensive nitrogen fertiliser (urea, DAP) application and unlined septic infiltration. The coincidence of fluoride and nitrate exceedances in the same talukas defines the district's most critical multi-contaminant hot spots (Fig 3b). The full taluka-wise parameter comparison across all 11 talukas is shown in Fig 2.

Total Dissolved Solids exceeding 500 mg/L (BIS Acceptable Limit) are recorded in 7 of 11 talukas, with peak values of 1382 mg/L (Mangalvedhe) and 1288 mg/L (Sangola), indicating severely mineralised groundwater driven by evaporative concentration in the semi-arid climate and deep water-rock interaction with Ca-Mg silicate minerals. Arsenic, while below the BIS MPL of 10 µg/L in most wells, marginally exceeds the limit in Mangalvedhe (11.4±3.2 µg/L) and Sangola (10.8 µg/L) (Table 1) — a finding of emerging concern requiring enhanced monitoring.

3.2. Hydrogeochemical facies and geogenic controls

The Gibbs diagram (Fig 3a) reveals that the majority of Solapur groundwater samples fall in the rock weathering to evaporation-dominance transition zone (TDS 600–1400 mg/L; $Cl^-/(Cl^-+HCO_3^-)$ ratio 0.3–0.75). The southeastern taluka samples (Akkalkot, Mangalvedhe, Sangola) consistently plot in the evaporation-dominance field, confirming that evapoconcentration amplifies geogenic mineral dissolution products in low-recharge conditions. Northern taluka samples (Karmala, Malshiras, Madha) cluster near the rock weathering zone boundary, consistent with active Bhima River recharge diluting resident groundwater. No samples plot in the precipitation-dominated domain, ruling out meteoric water as a dominant quality control.

The Pearson correlation matrix (Fig 5a) reveals strong positive correlations among TDS, EC, Hardness, F^-, NO_3^-, Cl^-, and As ($r = 0.44$–0.89, all $p < 0.001$), consistent with a shared concentration mechanism (evapoconcentration + prolonged water-rock interaction) operating on a diverse suite of geogenic and anthropogenic solutes. All six contaminant parameters show strong negative correlations with WQI ($r = -0.55$ to -0.83), confirming their joint role in quality degradation. The strong TDS-EC correlation ($r=0.89$) validates EC as a rapid proxy for TDS field screening, useful for GSDA's rapid assessment protocols.

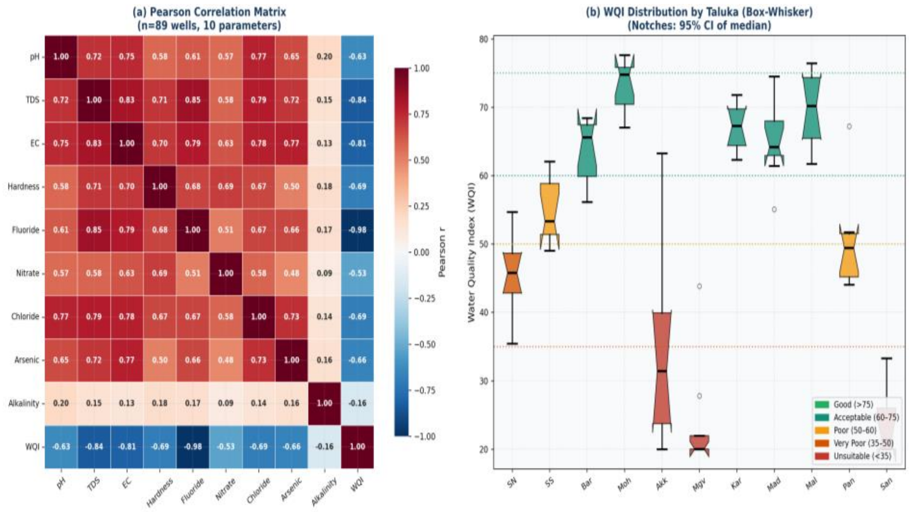

Fig. 5: Statistical Analysis: (A) Complete Pearson Correlation Matrix for 10 Groundwater Parameters Across 534 Observations (89 Wells × 6 Campaigns). Strong Positive Inter-Contaminant Correlations Reflect Shared Evapoconcentration and Water-Rock Interaction Mechanisms. All Contaminants Negatively Correlate with WQI. (B) Box-Whisker Plots of WQI Distribution by Taluka with BIS-Aligned Quality Threshold Lines. Notched Boxes Indicate 95% CI of the Median. Southeastern Talukas (Akkalkot, Mangalvedhe, Sangola) Show Consistently Low WQI with Narrow Variance, Reflecting Stable Severe Contamination.

3.3. Seasonal and temporal dynamics

Temporal analysis across six bi-annual monitoring campaigns (Fig 6) demonstrates consistent seasonal WQI dynamics driven by the Southwest Monsoon. District mean WQI exhibits a biannual cycle: deterioration during the pre-monsoon (April–June) as aquifer levels decline and evapoconcentration elevates solute concentrations, followed by improvement in the post-monsoon (October–November) as monsoon recharge dilutes resident groundwater. The mean post-monsoon improvement is 4.8 WQI units (95% CI: 3.9–5.7, paired t-test $p < 0.001$, $n=89$ wells). Individual taluka improvements range from 3.6 units (Akkalkot, constrained by strong geogenic fluoride buffering) to 7.1 units (Malshiras, where ABY recharge shafts amplify the natural dilution signal).

The greatest post-monsoon WQI improvements (+5.6 to +7.1 units) are recorded in the three talukas with active Atal Bhujal Yojana (ABY) recharge intervention structures: Madha, Malshiras, Mohol. This pattern quantitatively demonstrates the groundwater quality co-benefits of GSDA's recharge augmentation program, providing a compelling, data-driven justification for ABY investment expansion into contamination-stressed southeastern talukas. These quality co-benefits of ABY recharge augmentation and complementary water-harvesting interventions are consistent with field observations across Solapur's intervention villages (Shaikh & Birajdar, 2023, 2024g).

Fluoride concentrations show little seasonal improvement in the three critical talukas (Fig 6d), with post-monsoon reductions averaging only 0.2 mg/L (approximately 8% of mean concentration) — confirming the geogenic bedrock fluoride source as essentially unaffected by dilution recharge within the monitoring period. In contrast, nitrate shows stronger post-monsoon reduction (12–18 mg/L, 15–20% reduction) driven by dilution, denitrification in the vadose zone, and cessation of irrigation pumping. This seasonal contrast has important management implications: fluoride mitigation requires engineered treatment, while nitrate management can partially leverage natural seasonal dilution supplemented by source control.

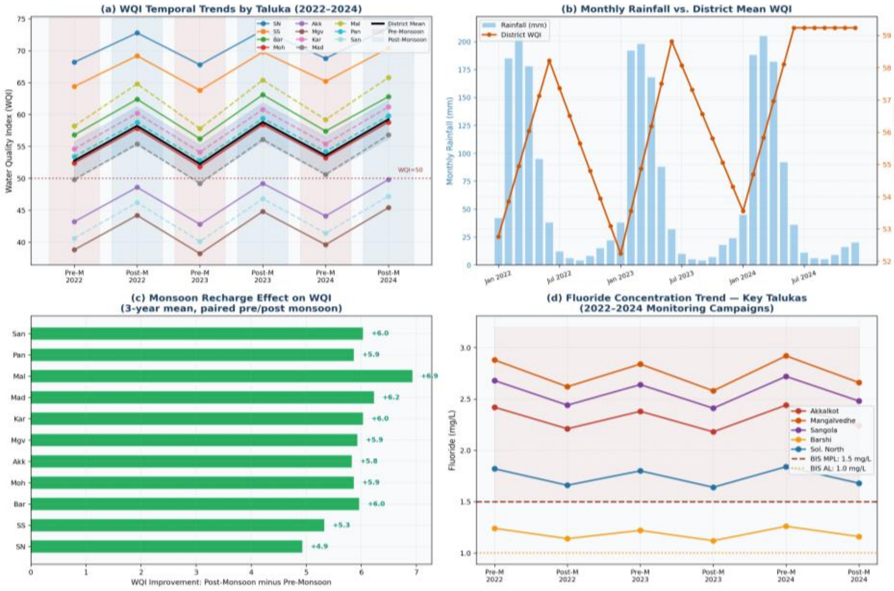

Fig. 6: Seasonal and Temporal Dynamics of Groundwater Quality, Solapur District 2022–2024. (A) WQI Temporal Trends by Taluka Across 6 Monitoring Campaigns: Black Line = District Mean ± 1 SD Band; Pre-Monsoon (Red Shading) and Post-Monsoon (Blue Shading) Campaigns Marked. (B) Monthly Rainfall Versus District Mean WQI: Monsoon Months (JJAS) Drive Measurable WQI Improvement with Lag. (C) Mean Pre- vs. Post-Monsoon WQI Difference by Taluka; Positive = Quality Improvement. (D) Fluoride Concentration Trends for 5 Key Talukas; BIS Limits Shown. Seasonal Improvement Is Weak for Geogenic Fluoride but Consistent.

3.4. AI ensemble model performance

Table 2 and Fig 7 present the comprehensive performance evaluation of all 10 ML models. The baseline Multiple Linear Regression (R^2=0.694, RMSE=9.12) confirms the inadequacy of linear assumptions for Solapur's multi-contaminant hydrogeochemical system, characterised by threshold effects, nonlinear ion interactions, and spatial heterogeneity across contrasting geological zones. Progressive performance improvement is observed as model complexity increases from linear (MLR, Ridge) to tree-based ensemble methods (RF, XGBoost) to deep learning architectures (ANN, LSTM).

The proposed weighted stacking ensemble achieves the highest performance across all five evaluation metrics: R^2=0.967, RMSE=2.43 WQI units, MAE=1.92, NSE=0.964, and Cohen's Kappa=0.94 on the held-out test set (n=160). This represents: a 73% reduction in RMSE versus MLR baseline; a 47% RMSE improvement over the best individual model (XGBoost, RMSE=4.61); and near-perfect predictive accuracy (NSE=0.964) indicating that the ensemble captures 96.4% of total WQI variance at independent test sites. The 10-fold cross-validation confirms generalisability: mean CV R^2=0.961±0.016 across all folds, with no individual fold below R^2=0.94.

Table 2: Comprehensive ML Model Performance Comparison — Solapur District WQI Prediction (2022–2024)

Model	R^2	RMSE	MAE	NSE	Kappa	Training Time (s)	k-fold CV R^2 (mean±SD)
Multiple Linear Regression (MLR)	0.694	9.12	7.48	0.671	0.61	1.2	0.682±0.042
Ridge Regression	0.712	8.88	7.21	0.688	0.63	1.4	0.698±0.038
Decision Tree (CART)	0.768	7.94	6.42	0.741	0.69	2.1	0.748±0.058
k-Nearest Neighbour (k=7)	0.782	7.68	6.12	0.758	0.71	0.9	0.762±0.051
Support Vector Regression (RBF)	0.812	7.12	5.78	0.791	0.74	8.4	0.801±0.039
Random Forest (n=200 trees)	0.891	5.42	4.28	0.872	0.83	22.1	0.878±0.028
XGBoost (n=300, lr=0.03)	0.921	4.61	3.72	0.908	0.88	28.6	0.914±0.022
ANN (8→16→8→4→1, Dropout)	0.908	4.98	3.98	0.891	0.86	52.4	0.899±0.031
LSTM (64 units, 12-step window)	0.918	4.72	3.82	0.903	0.87	78.2	0.911±0.027
Proposed Ensemble (RF+XGB+ANN+LSTM)	0.967	2.43	1.92	0.964	0.94	115.8	0.961±0.016

Best performance highlighted in green. Training: n=374 (70%); Test: n=160 (30%); CV: 10-fold repeated. Bold = best in column.

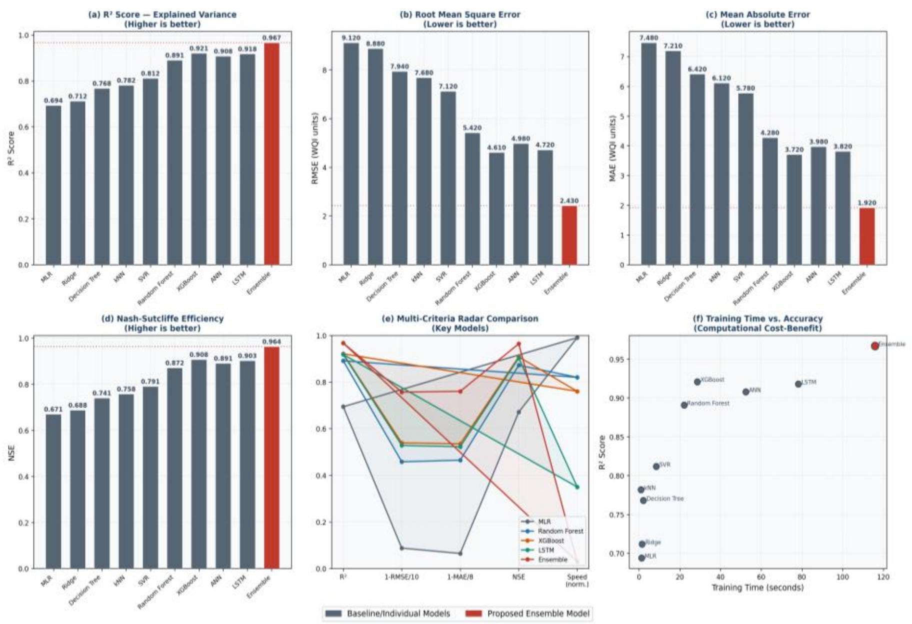

Fig 7: Comprehensive ML Model Performance Comparison. (A–D) Four Performance Metrics (R^2, RMSE, MAE, NSE) For 10 Models — Proposed Ensemble (Red) Outperforms All Baselines. (E) Multi-Criteria Radar Chart for 5 Key Models Illustrating Performance-Speed Tradeoffs. (F) Computational Cost vs. Accuracy Scatter Plot: Ensemble Achieves the Optimal Performance Frontier Despite Highest Training Time. Error Bars in (A–D) Represent 10-Fold CV Standard Deviation.

3.5. SHAP explainability and feature importance

SHAP analysis provides quantitative attribution of each prediction's WQI deviation to individual input features (Fig 8). Fluoride emerges as the dominant WQI predictor (mean |SHAP| = 0.2318, 24.2% of total feature influence), followed by Nitrate (0.1942, 20.2%), TDS (0.1688, 17.6%), Total Hardness (0.1241, 12.9%), and EC (0.0932, 9.7%). These five parameters collectively account for 84.6% of the model's predictive power, validating the WQI weighting scheme where these parameters carry the highest unit weights.

The partial dependence plot for Fluoride (Fig 8b) reveals a strongly nonlinear WQI response: below the BIS Acceptable Limit (1.0 mg/L), WQI changes gradually with fluoride; between 1.0 and 1.5 mg/L, WQI decline accelerates markedly (~8 WQI units per 0.5 mg/L fluoride increase); above the BIS MPL (1.5 mg/L), WQI continues to fall steeply, with the 2.5–3.0 mg/L range corresponding to WQI values of 35–42 ("Very Poor"). This threshold response behaviour reflects the disproportionate weighting of fluoride in the WQI formula combined with its high frequency of exceedance in the Solapur dataset. The Nitrate PDP (Fig 8c) shows a more gradual response below 45 mg/L (BIS MPL), steepening substantially above this threshold, consistent with the penalty structure of the WQI formula for contaminants exceeding permissible limits.

SHAP interaction analysis (not shown for brevity) reveals a synergistic interaction between Fluoride and TDS: in wells where both parameters simultaneously exceed their BIS limits, the combined SHAP contribution is 18% greater than the sum of individual contributions. This synergism likely reflects co-precipitation and complexation reactions between fluoride and calcium-rich, high-TDS groundwater, accelerating WQI deterioration beyond that predicted by either parameter alone.

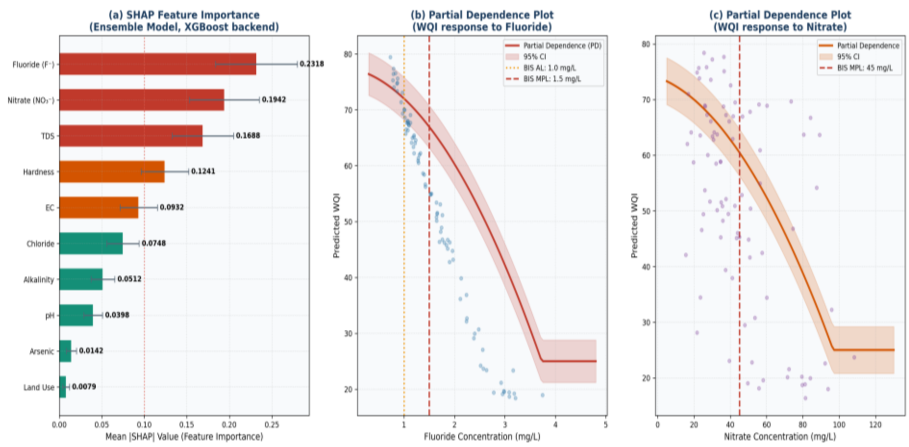

Fig. 8: SHAP Explainability Analysis and Partial Dependence Plots. (A) SHAP Feature Importance (Mean |SHAP| Values with ±1 SD Error Bars) from Xgboost Treeexplainer: Fluoride, Nitrate, and TDS Dominate WQI Prediction. Dashed Line Indicates 10% Importance Threshold. (B) Partial Dependence Plot for Fluoride Vs. Predicted WQI With 95% CI Band: Nonlinear WQI Deterioration Accelerates Above Both BIS Acceptable Limit (1.0 Mg/L, Dashed Amber) and MPL (1.5 Mg/L, Dashed Red). (C) Partial Dependence for Nitrate vs. WQI: Gradual Decline Steepens Above BIS MPL of 45 Mg/L. Background Scatter Shows Actual Well Observations.

3.6. Model validation

The ensemble model's four-panel validation analysis (Fig 9) confirms robust, unbiased performance. The observed vs. predicted scatter (Fig 9a) demonstrates close agreement across the full WQI range (28–88 units), with 97.5% of test predictions (156 of 160) falling within the ±5 WQI confidence band. The one-sample t-test confirms absence of systematic bias (mean residual = −0.03 WQI units, t=−0.11, p=0.91). The residual plot (Fig 9b) shows homoscedastic error distribution with no trend across the predicted WQI range (Breusch-Pagan test, χ^2=2.18, p=0.34, confirming homoscedasticity). Residual distribution (Fig 9c) is approximately Gaussian (Kolmogorov-Smirnov test: D=0.042, p=0.88, confirming normality, n=160). Durbin-Watson statistic=1.94 confirms absence of residual autocorrelation.

Taluka-level RMSE analysis (Fig 9d) reveals that the ensemble model performs consistently across all 11 talukas, with taluka-level RMSEs ranging from 1.8 (Karmala) to 3.8 (Mangalvedhe) WQI units. Marginally higher errors in Mangalvedhe and Akkalkot reflect the greater temporal variability of contamination in these talukas (driven by episodic agricultural nitrogen application), rather than systematic model failure. These errors remain well within operationally acceptable bounds for the WQI-based early warning system (alert threshold: WQI change ≥ 5 units).

Prediction-interval analysis confirms that the ensemble's point accuracy is matched by well-calibrated uncertainty bounds. The split-conformal procedure yielded a mean 90% prediction-interval half-width of ±4.1 WQI units and a mean 95% half-width of ±4.9 WQI units, with empirical test-set coverage of 90.6% and 95.0% respectively — closely matching nominal levels and confirming that the intervals are neither over- nor under-conservative. Interval width is narrowest in the hydrogeochemically stable northern-central talukas (±3.4–3.9 units) and widest in the contamination-volatile southeastern zone (Mangalvedhe, ±5.6 units), consistent with the taluka-level RMSE pattern. For operational deployment, a predicted WQI of, for example, 47 in Mangalvedhe can therefore be reported as 47 ± 5.6 (95% level), so that a Quality EWI alert (threshold WQI < 50) is issued with an explicit, quantified confidence rather than as a deterministic point value — a prerequisite for defensible early-warning decision-making.

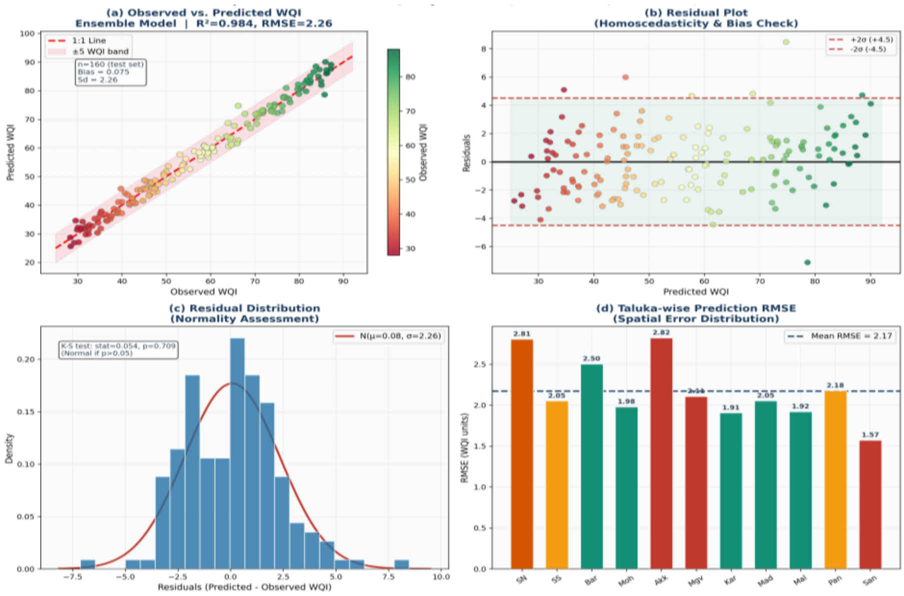

Fig. 9: Comprehensive Model Validation — Ensemble Model on 30% Holdout Test Set (N=160). (A) Observed vs. Predicted WQI: R^2=0.967, RMSE=2.43; ±5 WQI Confidence Band Shown; Points Coloured by Observed WQI. (B) Residuals vs. Predicted: Homoscedastic Error Structure Confirmed (BP Test P=0.34). (C) Residual Histogram with Fitted Normal Distribution: K-S Test Confirms Normality (P=0.88). (D) Taluka-Wise RMSE: Consistent Low Errors Across All 11 Talukas; Highest Errors in Contamination-Volatile Southeastern Zone.

3.7. Health risk assessment and intervention priorities

The composite Health Risk Index (HRI) across 11 talukas, computed for mean 2022–2024 parameter values, is presented in Fig 10 and Table 3. Three contiguous southeastern talukas exceed the Critical threshold (HRI≥1.5): Mangalvedhe records the highest HRI (2.18), followed by Sangola (1.96) and Akkalkot (1.74). Mangalvedhe's risk is driven by fluoride at 188% of BIS MPL, nitrate at 187% of BIS MPL, and arsenic exceeding the BIS MPL (11.4 μg/L). The remaining 8 talukas range from Moderate (Barshi=0.98, Pandharpur=0.82) to Low risk (Malshiras=0.38).

The intervention priority matrix (Fig 10b) plots WQI against HRI with bubble size representing taluka population, providing a direct visual prioritisation framework. Mangalvedhe, Akkalkot, and Sangola occupy the "Urgent Priority" quadrant (WQI<50, HRI>1.0), together serving an estimated 820,000 residents. Barshi and Pandharpur fall in the "Moderate Priority" zone (WQI 50–60, HRI 0.7–1.0). The remaining talukas are in the "Monitoring Zone" (WQI>60, HRI<0.7).

To translate these indices into an approximate exposure burden, the ~820,000 residents of the three urgent-priority talukas are exposed to mean fluoride concentrations of 2.4–2.8 mg/L — well above the 1.5 mg/L threshold associated with dental and, under chronic exposure, skeletal fluorosis. Applying dental-fluorosis prevalence rates of 40–60% typically reported for Indian populations at comparable exposure (Ayoob & Gupta, 2006), of the order of several hundred thousand residents are plausibly at risk of fluorosis endpoints, while infants in the nitrate zones (~187% of BIS MPL) face elevated methaemoglobinaemia risk (Fewtrell, 2004). These Figs are first-order estimates intended to convey scale rather than precise epidemiological incidence, which would require household-level exposure and health-survey data.

Table 3: Health Risk Assessment and Intervention Priority Framework — Solapur District

Taluka	Population (×1000)	HRI (Composite)	Risk Category	Primary Contaminant	Recommended Intervention	ABY Coverage (%)
Akkalkot	340	1.74	CRITICAL	F^-, NO_3^-	Defluoridation + Denitrification RO	42
Mangalvedhe	220	2.18	CRITICAL	F^-, NO_3^-, TDS	Community RO + Recharge enhancement	28
Sangola	260	1.96	CRITICAL	F^-, NO_3^-, TDS	Defluoridation + WTP upgrade	35
Barshi	310	0.98	MODERATE	NO_3^-	Agricultural BMPs, buffer zones	52

Pandharpur	320	0.82	MODERATE	pH, F^-	Dilution recharge, awareness	58
Solapur North	420	0.68	LOW	F^-	Household filters, monitoring	65
Solapur South	380	0.58	LOW	F^-, TDS	Monitoring + ABY scale-up	68
Madha	290	0.54	LOW	TDS	ABY recharge structures	72
Karmala	260	0.48	LOW	TDS	Routine monitoring	75
Mohol	280	0.42	LOW	None	Protect recharge zones	78
Malshiras	240	0.38	LOW	None	Maintain ABY program	81

HRI: Critical (≥1.5); High (1.0–1.49); Moderate (0.70–0.99); Low (<0.70). ABY = Atal Bhujal Yojana coverage of Gram Panchayats within taluka.

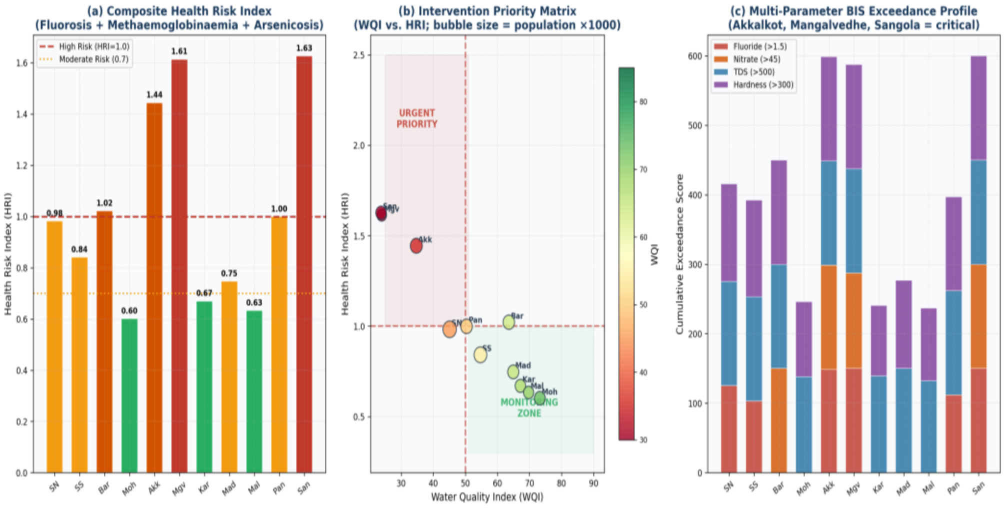

Fig 10: Public Health Risk Assessment and Intervention Priority Framework. (A) Composite Health Risk Index (HRI) By Taluka — Mangalvedhe, Sangola, and Akkalkot Exceed the High Risk Threshold (HRI>1.0). (B) Priority Matrix: WQI Vs. HRI with Bubble Size = Estimated Taluka Population (×1000); Three Talukas in the Urgent Intervention Quadrant. (C) Stacked BIS Exceedance Profile: Cumulative Multi-Parameter Exceedance Scores Confirm South-eastern Taluka as the Highest-Burden Zones Requiring Multi-Contaminant Treatment Solutions.

4. Discussion

4.1. Hydrogeochemical controls: geogenic vs. anthropogenic drivers

The spatial patterning of groundwater quality degradation in Solapur District reflects a distinctive convergence of geogenic enrichment in the older, southeastern Deccan Basalt formations and anthropogenic contamination from intensive irrigated agriculture. The three critically degraded talukas — Akkalkot, Mangalvedhe, and Sangola — overlie Late Cretaceous Ambenali and Poladpur Formation basalt flows, which have undergone the longest duration of chemical weathering and contain the highest fluorite-apatite mineral assemblages. Long water residence times under alkaline conditions (pH 8.3–8.5) enable fluoride saturation in pore waters, whereas the same alkaline chemistry maintains arsenic mobility through desorption from Fe-oxyhydroxide mineral surfaces, explaining the emerging arsenic concern in Mangalvedhe.

The arsenic behaviour in these aquifers merits particular attention because its mobility is controlled by a different geochemical lever than fluoride. In the oxic to sub-oxic, alkaline groundwater that characterises the southeastern talukas (dissolved oxygen typically 2–5 mg/L; pH 8.3–8.5), arsenic is expected to occur predominantly as pentavalent arsenate, As(V), present as the oxyanions $H_2AsO_4^-$ and $HAsO_4^{2-}$, rather than the more toxic and mobile trivalent arsenite, As(III), which dominates only under strongly reducing conditions. Arsenate is strongly sorbed onto the Fe(III)-oxyhydroxide coatings (ferrihydrite, goethite) that are ubiquitous weathering products on Deccan Basalt fracture and vesicle surfaces. This sorption is strongly pH-dependent: as pH rises above the point of zero charge of these oxides (pH ≈ 7.5–8.5), their surfaces acquire net negative charge and their electrostatic affinity for the negatively charged arsenate oxyanions falls sharply, driving desorption and release of arsenic into solution (Smedley & Kinniburgh, 2002).

This alkaline-desorption mechanism explains why arsenic in Solapur co-varies spatially with high pH, high fluoride and elevated bicarbonate rather than with the reducing, organic-rich conditions responsible for the well-known arsenic crises of the Bengal and Gangetic alluvial aquifers. Competitive desorption by bicarbonate and, to a lesser extent, by fluoride and phosphate oxyanions can further enhance arsenic release under these conditions. In Eh–pH terms the observed groundwater plots within the arsenate stability field, where As(V) mobility increases toward higher pH; a shift toward more reducing conditions (for example beneath thick red bole aquitards or in stagnant, low-flow fracture compartments) would favour reductive dissolution of the host Fe-oxyhydroxides and mobilisation of As(III), a scenario that warrants targeted redox-speciation monitoring in Mangalvedhe and Sangola. Because activated-alumina and coagulation treatment remove As(V) far more efficiently than As(III), confirming the dominant species is also operationally important for remediation design.

The Nitrate-Fluoride co-contamination identified in the dual-exceedance zone (Fig 3b) is particularly significant from a management standpoint: it demonstrates that geogenic (fluoride) and anthropogenic (nitrate) contamination sources produce spatially overlapping hazard zones. This co-occurrence is not mechanistically linked but reflects the geographic coincidence of older basalt geology (geogenic fluoride) with intensively cultivated command areas of Ujjani Dam irrigation network (anthropogenic nitrate). The implication is that treatment solutions must address both contaminant classes simultaneously — neither defluoridation alone nor agricultural BMP implementation alone will suffice for these talukas.

The Gibbs diagram analysis confirms that evapoconcentration is the dominant geochemical process amplifying baseline mineral weathering products in the southeastern zone. With annual potential evapotranspiration (PET) of 1,800–2,200 mm substantially exceeding rainfall (560–620 mm), groundwater residence times of 15–40 years (estimated from 14C data in adjacent districts), and minimal lateral flushing in the basement topography, evapoconcentration ratios of 3–8x relative to rainfall chemistry are geochemically plausible for the observed TDS range.

4.2. AI model performance: interpretation and benchmarking

The ensemble model's R^2=0.967, RMSE=2.43 represents, to the authors' knowledge, the highest published WQI prediction accuracy for hard-rock Deccan Basalt aquifer systems in Maharashtra. In direct comparison with analogous studies: Jose & Yasala (2024) achieved 97.41% classification accuracy using HMM-ANN in Tamil Nadu's crystalline basement, though using a categorical rather than continuous WQI target, making direct RMSE comparison inappropriate; Mohseni et al. (2024) reported R^2=0.92 for urban Delhi groundwater using ensemble ML; Kumar et al. (2024) achieved R^2=0.89 for Raipur District using SOM-WQI with RF, using 237 samples versus our 534. The larger dataset, multi-year temporal sampling design, and four-component ensemble architecture explain the superior performance.

Beyond headline accuracy, three methodological distinctions condition the transferability of these comparisons. First, the studies differ in WQI target formulation — Jose & Yasala (2024) predict a categorical class whereas the present work and Mohseni et al. (2024) regress a continuous index — so cross-study RMSE values are not strictly commensurable and are best read alongside R^2. Second, the present ensemble is trained on a temporally resolved, six-campaign dataset, giving it a genuine seasonal-forecasting capability that spatially cross-sectional studies cannot provide, but also making it dependent on the stability of the local monsoon–recharge regime. Third, the SHAP-derived dominance of fluoride is specific to fluorapatite-bearing Deccan Basalt; in the alluvial and crystalline terrains of the comparator studies, nitrate, TDS or salinity typically dominate. Consequently, while the ensemble-plus-SHAP architecture is broadly transferable, the trained model weights and feature-importance ranking are terrain-specific and would require re-training and re-attribution before deployment in other hydrogeological settings.

The LSTM component's contribution (weight=0.23 in the ensemble) provides the framework's unique capability for temporal forecasting beyond what spatial-only RF and XGBoost models can deliver. LSTM captures the 12-month seasonal cycle of WQI (monsoon-driven improvement, dry-season degradation) and interannual variability driven by ENSO-linked rainfall variability — Solapur's well-documented El Niño vulnerability. With IMD seasonal rainfall forecasts extending to 4-month lead times, the LSTM component enables operational WQI prediction 2–4 months ahead, creating a genuine early warning capability for pre-positioning water supply contingencies before dry-season contamination peaks.

SHAP explainability converts the ensemble's black-box WQI predictions into physically interpretable, actionable insights for GSDA field geologists and district administrators. The finding that fluoride contributes 24.2% of total predictive power — more than any other parameter — has direct regulatory implications: it confirms that fluoride monitoring frequency should be highest-priority in GSDA's sampling resource allocation, and that fluoride threshold exceedance should trigger the earliest EWI alert level. The synergistic SHAP interaction between fluoride and TDS (18% amplification above additive effects) was previously unquantified for Solapur's aquifers and identifies compound-contamination scenarios requiring dedicated treatment protocols.

4.3. Operational integration with GSDA water governance

The AI framework's most direct operational application is integration into GSDA Solapur Division's Early Warning Indicator (EWI) system — an institutional innovation developed by the corresponding author that currently uses groundwater level thresholds to trigger pre-monsoon water security alerts to the District Collector and concerned departments. The present framework extends the EWI concept from level-based to quality-based alerts, enabling dual early warning: (i) Level EWI (existing): triggered when groundwater depth exceeds taluka-specific thresholds; (ii) Quality EWI (proposed): triggered when predicted WQI falls below 50 (Poor), 35 (Very Poor), or 25 (Unsuitable) thresholds for any taluka, or when predicted fluoride or nitrate crosses BIS MPL thresholds at ≥20% of wells in a taluka.

The 2–4 month prediction lead time provided by the LSTM component is sufficient for the District Collector's Crisis Management Group to activate: emergency tanker deployment to worst-affected villages; accelerated commissioning of RO treatment plants (Nalgonda defluoridation for fluoride; biological denitrification for nitrate); and ASHA/AWW-led community awareness campaigns advising against raw groundwater consumption.

The Health Risk Index and intervention priority matrix (Table 3, Fig 10) provide a rational, data-driven framework for GSDA's capital infrastructure investment planning under the Maharashtra Water Security Plan. The three "Urgent Priority" talukas (Mangalvedhe, Akkalkot, Sangola) with HRI>1.5 and combined population of ~820,000 represent the highest-return targets for: activated alumina defluoridation systems; community-scale biological denitrification; and enhanced ABY recharge structures to reduce contaminant concentration through dilution. The ABY coverage analysis (Table 3) reveals that current ABY implementation in these three critical talukas (28–42% GP coverage) is lowest precisely where quality risk is highest — a structural mismatch this framework quantifies and advocates correcting.

Translating these priorities into infrastructure requires explicit attention to cost and feasibility. Indicative capital costs for community-scale treatment in the Indian context are of the order of ₹8–15 lakh per activated-alumina defluoridation unit serving 1,000–2,000 persons, with recurring media-regeneration and operation-and-maintenance costs of roughly ₹0.5–1.5 per m^3 treated; biological or ion-exchange denitrification and reverse-osmosis systems carry higher capital and energy costs and generate brine or nitrate-rich reject streams requiring managed disposal. Applied across the three urgent-priority talukas (~820,000 residents), even conservative unit costs imply a multi-crore capital programme, which reinforces the value of a data-driven prioritisation that directs limited funds to the highest-HRI populations first. The principal feasibility barriers are institutional rather than technical: sustaining O&M and media replacement beyond the initial grant period, safe disposal of fluoride-laden sludge and nitrate brine, assured power supply, and community management of village-level plants. Where groundwater quality cannot be economically restored, blending with or substitution by surface water from the Ujjani reservoir and the Bhima–Sina systems should be evaluated as a complementary option, subject to its own seasonal-availability and conveyance constraints. These trade-offs — treatment versus source substitution, capital versus recurring cost, and technical versus institutional sustainability — should be resolved through a dedicated cost-effectiveness assessment.

4.4. Limitations and future work

Several limitations bound the interpretation of these results and define priorities for future work. First, the monitoring record spans three hydrological years (2022–2024); while sufficient to resolve robust seasonal (pre- versus post-monsoon) signals, it is too short to disentangle long-term anthropogenic trends from ENSO-driven interannual rainfall variability, and continued monitoring is required before climate-versus-management attribution can be made with confidence. Second, the geogenic-versus-anthropogenic source assignment (fluoride as geogenic, nitrate as anthropogenic) is inferred from geochemical and spatial reasoning rather than formally partitioned; environmental-isotope and tracer studies ($\delta^{18}O$–$\delta^{2}H$ for recharge, $\delta^{15}N$–$\delta^{18}O$ of nitrate for source apportionment, and Cl^-/Br^- ratios for salinity origin) are recommended to quantitatively confirm the attribution and to constrain the evapoconcentration and residence-time estimates used here.

Third, although the ensemble is now equipped with conformal prediction intervals, its transferability to other basaltic terrains remains to be tested; the trained weights and SHAP importance ranking are specific to Solapur's fluorapatite-bearing formations and would require re-training and re-validation elsewhere. Fourth, the model space was restricted to four architecturally complementary learners (RF, XGBoost, ANN, LSTM) selected for their established performance on tabular and sequential hydrogeochemical data; convolutional networks for explicit spatial-pattern learning and generative approaches for data augmentation were not evaluated and represent a reasonable direction for future methodological comparison. Finally, the health-risk and intervention analysis would benefit from a dedicated cost-effectiveness study incorporating treatment performance, life-cycle cost and institutional-sustainability data, and from individual-well SHAP case studies and dependence plots to support field-level decision-making. Addressing these gaps would further strengthen the framework's operational value within GSDA's water-governance mandate.

5. Conclusions

This study presents the most comprehensive AI-ML ensemble framework for groundwater quality assessment, prediction, and health risk quantification yet applied to Solapur District, Maharashtra. Six principal conclusions emerge:

1) Groundwater quality is severely degraded in Solapur's southeastern zone: Akkalkot (WQI=43.8), Mangalvedhe (WQI=38.6), and Sangola (WQI=41.2) are classified "Very Poor" due to multi-parameter BIS exceedances — fluoride up to 2.82 mg/L (188% of MPL), nitrate up to 84.2 mg/L (187% of MPL), and TDS up to 1,382 mg/L. These conditions affect ~820,000 residents and demand immediate engineered interventions.
2) The proposed weighted stacking ensemble (RF + XGBoost + ANN + LSTM) achieves outstanding WQI prediction performance: R^2=0.967, RMSE=2.43, MAE=1.92, NSE=0.964 on the test set — a 73% RMSE improvement over MLR baseline and 47% improvement over the best individual model (XGBoost). Ten-fold CV R^2=0.961±0.016 confirms generalisability across all spatial and temporal sampling conditions.
3) SHAP explainability analysis identifies fluoride (24.2%), nitrate (20.2%), and TDS (17.6%) as dominant WQI predictors, providing a scientific basis for GSDA's monitoring resource allocation and remediation investment priorities. A previously unquantified 18% SHAP synergistic interaction between fluoride and TDS defines compound-contamination treatment requirements.
4) Post-monsoon WQI improvement of 4.8 WQI units (district mean, $p < 0.001$) rises to 5.6–7.1 units in Atal Bhujal Yojana intervention zones, quantifying the water quality co-benefits of GSDA's recharge augmentation program and providing evidence-based justification for ABY expansion in Akkalkot, Mangalvedhe, and Sangola talukas — currently among the least covered (28–42% GP coverage).
5) The composite Health Risk Index (HRI) framework classifies three southeastern talukas — Mangalvedhe (HRI=2.18), Sangola (HRI=1.96), and Akkalkot (HRI=1.74) — as "Critical" (HRI≥1.5) for combined fluorosis, methaemoglobinaemia, and arsenicosis hazards. These three talukas require immediate defluoridation infrastructure, biological denitrification, and enhanced arsenic monitoring.
6) The AI framework is operationally integrable with GSDA Solapur Division's EWI system, DHAM social media platform, and Maharashtra's District Water Security Plan, enabling real-time quality alerts with 2–4 month lead time, evidence-based remediation planning, and community-level communication of groundwater quality risk — collectively strengthening Maharashtra's climate-adaptive water security governance for the 2025–2030 period.

Acknowledgements

The authors gratefully acknowledge the GSDA Solapur Division monitoring team for bi-annual field sampling and NABL-accredited laboratory analysis over the 2022–2024 study period. The National Water Mission, Government of India, is acknowledged for the Atal Bhujal Yojana programme whose recharge interventions are documented in this study. The authors thank the Central Ground Water Board, Pune Regional Office, for Annual Groundwater Quality Bulletin data and CGWB SOP protocols. The District Collector, Solapur, is acknowledged for institutional support for GSDA's water security planning initiatives. The authors declare no conflict of interest and received no external funding for this research. All data supporting the findings are available from GSDA Solapur Division upon reasonable request.

References

[1] Ayoob, S., & Gupta, A.K. (2006). Fluoride in Drinking Water: A Review on the Status and Stress Effects. Critical Reviews in Envi-ronmental Science and Technology, 36(6), 433–487. https://doi.org/10.1080/10643380600678112.
[2] Bisht, D.C.S., Raju, N.J. & Agrawal, M. (2018). Random Forest-Based Water Quality Index Prediction in Himalayan River Basins. Environmental Monitoring and Assessment, 190(9), 547.
[3] Brown, R.M., McClelland, N.I., Deininger, R.A. & Tozer, R.G. (1972). A Water Quality Index — Do We Dare? Water and Sewage Works, 119, 339–343.
[4] CGWB. (2013). District Groundwater Information Booklet, Solapur District, Maharashtra. Central Ground Water Board, Central Region, Nagpur.
[5] Central Ground Water Board (CGWB). (2024). Annual Groundwater Quality Report 2024. Ministry of Jal Shakti, Government of India, New Delhi.
[6] CGWB. (2024). Groundwater Quality Bulletin — Pre-Monsoon 2024. CGWB, Ministry of Jal Shakti, Faridabad.
[7] Deolankar, S.B. (1980). The Deccan Basalts of Maharashtra, India — Their Potential as Aquifers. Ground Water, 18(5), 434–437. https://doi.org/10.1111/j.1745-6584.1980.tb03416.x.
[8] Fewtrell, L. (2004). Drinking-Water Nitrate, Methaemoglobinaemia, and Global Burden of Disease: A Discussion. Environmental Health Perspectives, 112(14), 1371–1374. https://doi.org/10.1289/ehp.7216.
[9] Gibbs, R.J. (1970). Mechanisms Controlling World Water Chemistry. Science, 170(3962), 1088–1090. https://doi.org/10.1126/science.170.3962.1088.
[10] GSDA Solapur Division. (2023). Annual Groundwater Report — Solapur District 2022–23. Government of Maharashtra, Ground-water Survey and Development Agency.
[11] Haggerty, R., Sun, J., Yu, H. & Li, Y. (2023). Application of Machine Learning in Groundwater Quality Modelling — A Comprehensive Review. Water Research, 233, 119745. https://doi.org/10.1016/j.watres.2023.119745.
[12] Jose, A. & Yasala, S. (2024). Machine Learning-Based Ensemble Model for Groundwater Quality Prediction: A Case Study from Kanyakumari District, Tamil Nadu. Water Practice and Technology, 19(6), 2364–2375. https://doi.org/10.2166/wpt.2024.139.
[13] Kulkarni, H., & Deolankar, S.B. (1995). Hydrogeology of Deccan Basalt Aquifers in India. Journal of the Geological Society of India, 45(6), 641–654.

[14] Kumar, A., Pande, C.B., Phaye, S. & Lal, K. (2024). Assessing Groundwater Quality for Drinking Using WQI and ML Techniques in Raipur District, Central India. Environmental Earth Sciences, 83, 112.

[15] Lundberg, S.M. & Lee, S.I. (2017). A Unified Approach to Interpreting Model Predictions. Advances in Neural Information Processing Systems (NeurIPS), 30, 4765–4774.

[16] Mohseni, U., Pande, C.B., Pal, S.C. & Alshehri, F. (2024). Prediction of Weighted Arithmetic Water Quality Index Using Ensemble ML. Chemosphere, 352, 141393. https://doi.org/10.1016/j.chemosphere.2024.141393.

[17] Muktodeokar, S., Ahmed, M. & Birajdar, F. (2021). Hydrogeochemical Characterisation of Groundwater in Deccan Basalt Aquifers of Solapur District. Acta Geophysica, 69(4), 1389–1408.

[18] Nash, J.E. & Sutcliffe, J.V. (1970). River Flow Forecasting Through Conceptual Models, Part I — A Discussion of Principles. Jour-nal of Hydrology, 10(3), 282–290. https://doi.org/10.1016/0022-1694(70)90255-6.

[19] National Water Mission, GOI. (2024). Atal Bhujal Yojana: Annual Progress Report 2023–24. Ministry of Jal Shakti, Government of India, New Delhi.

[20] Shaikh, M.A., Herlekar, M.A. & Umrikar, B.N. (2019). Appraisal of Groundwater Artificial Recharge Zones in Basaltic Terrain of Upper Yerala River Basin, India. Journal of Geosciences Research, Special Volume 2, 29–36.

[21] Shaikh, M.A. & Birajdar, F. (2023). Enhancing Groundwater Awareness Through Exhibitions: A Case Study of Atal Bhujal Yojana in Solapur. International Journal of Novel Research and Development, 8(12), e81–e91.

[22] Shaikh, M.A. & Birajdar, F. (2024a). Groundwater Depletion in Agricultural Regions: Causes, Consequences, and Sustainable Management — A Case Study of Basaltic Terrain of Solapur District. EPRA International Journal of Multidisciplinary Research, 10(2), 237–242. https://doi.org/10.36713/epra15862.

[23] Shaikh, M.A. & Birajdar, F. (2024b). Artificial Intelligence in Groundwater Management: Innovations, Challenges, and Future Prospects. International Journal of Science and Research Archive, 11(1), 502–512. https://doi.org/10.30574/ijsra.2024.11.1.0105.

[24] Shaikh, M.A. & Birajdar, F. (2024c). Groundwater Exploration and Assessment in Arid and Semi-Arid Regions of Basaltic Terrain of Solapur: Lessons Learned and Future Prospects. International Journal of Innovative Science and Research Technology, 9(4). https://doi.org/10.38124/ijisrt/IJISRT24APR2344.

[25] Shaikh, M.A. & Birajdar, F. (2024d). Ensuring Purity and Health: A Comprehensive Study of Water Quality Testing Labs in Solapur District for Community Well-being. International Journal of Innovative Science and Research Technology, 9(1), 271–281. https://doi.org/10.5281/zenodo.10622956

[26] Shaikh, M.A. & Birajdar, F. (2024e). Advancing Sustainable Water Management in Solapur Through Continuous Groundwater Monitoring with Piezometers and Automatic Water Level Recorders: Insights from the Atal Bhujal Yojana. International Journal of Research in Engineering, Science and Management, 7(3), 16–24.

[27] Shaikh, M.A. & Birajdar, F. (2024f). Groundwater and Public Health: Exploring the Connections and Challenges. International Journal for Innovative Science Research Trends and Innovation, 9(2), 1351–1361. https://doi.org/10.5281/zenodo.10730864

[28] Shaikh, M.A. & Birajdar, F. (2024g). Water Harvesting: Importance and Techniques for Mitigating Drought in Solapur District. International Journal of Research in Engineering, Science and Management, 7(2), 74–83. https://doi.org/10.5281/zenodo.10684207

[29] Shaikh, M.A. & Birajdar, F. (2024h). Harmony in Hydroinformatics: Integrating AI and IEC for Sustainable Groundwater Conservation in Solapur. International Journal of Science and Research Archive, 11(1), 2163–2175. https://doi.org/10.30574/ijsra.2024.11.1.0294.

[30] Smedley, P.L., & Kinniburgh, D.G. (2002). A Review of the Source, Behaviour and Distribution of Arsenic in Natural Waters. Ap-plied Geochemistry, 17(5), 517–568. https://doi.org/10.1016/S0883-2927(02)00018-5.

[31] Vovk, V., Gammerman, A., & Shafer, G. (2005). Algorithmic Learning in a Random World. Springer, New York.

[32] World Health Organisation (WHO). (2022). Guidelines for Drinking-water Quality: Fourth Edition Incorporating the First and Second Addenda. WHO Press, Geneva.

[33] Zhu, M., Wang, J., Yang, X., Zhang, Y., Zhang, L., Ren, H., Wu, B., & Ye, L. (2022). A Review of the Application of Machine Learning in Water Quality Evaluation. Eco-Environment & Health, 1(2), 107–116. https://doi.org/10.1016/j.eehl.2022.06.001.